Precise stellar ages: combining isochrone fitting with empirical gyrochronology

Ruth Angus[1,2,], Timothy D. Morton[3,2,], Dan Foreman-Mackey[2], Jason Curtis[4], Stephen Kane[5], Megan Bedell[2], John Brewer[9], Jen van Saders[11], David W. Hogg[6,2,8] Rocio Kiman[10,1]

ABSTRACT

[1]American Museum of Natural History, Central Park West, Manhattan, NY, USA

[2]Center for Computational Astrophysics, Flatiron Institute, 162 5th Avenue, Manhattan, NY, USA

[3]Department of Astronomy, University of Florida, Gainesville, FL, USA

[4]Department of Astronomy, Columbia University, Manhattan, NY, USA

[5]Department of Physics and Astronomy, UC Riverside, Riverside, CA, USA

[6]Center for Cosmology and Particle Physics, New York University, Manhattan, NY, USA

[7]Center Data Science, New York University, Manhattan, NY, USA

[8]Max-Planck Institute for Astronomy, Königstuhl, Heidelberg, Germany

[9]Yale center for astronomy and astrophysics, Yale University, New Haven, CT, USA

[10]Department of physics, CUNY Graduate Center, City University of New York, Manhattan, NY, USA

[11]Institute for Astronomy, University of Hawai'i at Mānoa, Honolulu, HI, USA

We present a new age-dating technique that combines gyrochronology and isochrone fitting to infer ages for AFGKM main-sequence and subgiant field stars. The age-dating methods of gyrochronology and isochrone fitting are each capable of providing relatively precise ages in certain areas of the Hertzsprung-Russell diagram: rotation periods can provide precise ages for cool stars on the main sequence via gyrochronology, and isochrone fitting can provide precise ages for stars near main sequence turn off. Combined, these two age-dating techniques can be applied to a broader range of stellar masses and evolutionary stages and can provide ages that are more precise and accurate than either method used in isolation. In this investigation, we demonstrate that the position of a star on the Hertzsprung-Russell or color-magnitude diagram can be combined with its *Kepler* rotation period to infer a precise age via both isochrone fitting and gyrochronology simultaneously. We show that incorporating rotation periods into stellar evolution models particularly improves age precision and accuracy for GK stars on the main sequence, and can result in age estimates that are three times more precise and accurate than isochrone fitting alone for these stars. In addition, we provide a new gyrochronology relation, calibrated to the Praesepe cluster and the Sun, that includes a variance model to capture the rotational behavior of stars without Sun-like magnetic dynamos. This publication is accompanied by an open source *Python* package (`stardate`) for inferring the ages of main sequence and subgiant AFGKM stars from rotation periods, spectroscopic parameters and/or apparent magnitudes and parallaxes.

1. Introduction

Age is the most difficult stellar property to measure, and the difficulty of age-dating is particularly acute for low mass (GKM) stars on the main sequence (MS). Using conventional dating methods, uncertainties on the ages of these stars can be as large as the age of the Universe. GKM dwarfs are difficult to age-date because their physical and observable properties do not change rapidly. This is represented in the spacing of isochrones on a Hertzsprung-Russell diagram (HRD) or color-magnitude diagram (CMD). On the MS, isochrones are tightly spaced and, even with very precise measurements of effective temperature and luminosity, the position of a MS star on the HRD may be consistent with range of isochrones spanning several billion years. At main sequence turn-off however, isochrones are

spread further apart, so that sufficiently precisely measured temperatures and luminosities can yield ages that are extremely precise (*e.g.* Pont and Eyer 2004). The classical method for measuring stellar ages is isochrone placement, or isochrone fitting, where surface gravity changes resulting from fusion in the core (usually observed via luminosity, L, and effective temperature, $T_{\rm eff}$, or absolute magnitude and colour) are compared with a set of models that trace stellar evolution across the HRD, or CMD. CMD/HRD position has been thoroughly mapped with physical models, and can be used to calculate relatively accurate (but not necessarily precise) ages, barring some small, $\sim 10\%$ variations between different models, (*e.g.* Yi et al. 2001; Dotter et al. 2008; Dotter 2016). On the MS itself, there is little differentiation between stars of different ages in the L and $T_{\rm eff}$ plane, so ages tend to be very imprecise. The method of inferring a star's age from its rotation period, called 'gyrochronology', is much better suited for measuring ages on the MS because MS stars spin down relatively rapidly.

Magnetic braking in MS stars was first observed by Skumanich (1972) who, studying young clusters and the Sun, found that the rotation periods of Solar-type stars decay with the square-root of time. It has since been established that the rotation period of a MS star depends, to first order, only on its age and effective temperature or color (*e.g.* Barnes 2003). The convenient characteristic of stars that allows their ages to be inferred from their *current* rotation periods and independently of their primordial ones, comes from the steep dependence of spin-down rate on rotation period (Kawaler 1989). Stars spinning with high angular velocity will experience a much greater angular momentum loss rate than slowly spinning stars and for this reason, no matter the initial rotation period, Solar type stars will have the same rotation period after around the age of the Hyades, 500-700 million years (Irwin and Bouvier 2009; Gallet and Bouvier 2015). After this time, the age of a star can be inferred, to first order, from its dust-corrected color (*e.g.* B-V or $G_{BP} - G_{RP}$) and rotation period alone and this is the principle behind gyrochronology.

The relation between age, rotation period and mass has been studied in detail, and several different models have been developed to capture the rotational evolution of Sun-like stars. Some of these models are theoretical and based on physical processes; modeling angular momentum loss as a function of stellar properties as well as the properties of the magnetic field and stellar wind (*e.g.* Kawaler 1988, 1989; van Saders and Pinsonneault 2013; Matt et al. 2015; van Saders et al. 2016). Other models are empirical and capture the behavior of stars from a purely observational standpoint, using simple functional forms that can reproduce the data (*e.g.* Barnes 2003, 2007; Mamajek and Hillenbrand 2008; Angus et al. 2015). Both types of model, theoretical and empirical, must be calibrated using observations. Old calibrators are especially important because new evidence suggests that rotational evolution goes through a transition at old age or, more specifically, at a large Rossby number, Ro (the ratio of rotation period to the convective overturn timescale). For example, stars shown to

be old from *Kepler* asteroseismic data rotate more rapidly than expected given their age (Angus et al. 2015; van Saders et al. 2016). A new physically motivated gyrochronology model, capable of reproducing these data, was recently introduced (van Saders et al. 2016). It relaxes magnetic breaking at a critical Rossby number of around 2, approximately the Solar value. This model predicts that, after stellar rotation periods lengthen enough to move stars across this Ro threshold, stars stop spinning down and maintain a constant rotation period from then until they evolve off the MS. As demonstrated in section 3 however, this does not mean that the ages of stars with Ro > 2 cannot be measured from their rotation periods, especially if their rotation periods are combined with HRD or CMD placement.

The gyrochronology models that capture post Ro-threshold, rotational evolution (van Saders et al. 2016) are the current state-of-the-art in rotation dating. These models can be computed over a grid of stellar parameters, and interpolated over to predict the age of a star. The process of measuring the age of a field star with these models is similar to inferring an age using any set of isochrones, with difference that rotation period is an additional observable dimension. Ages calculated using these models are therefore likely to be much more precise than using rotation-free isochrones since rotation period provides an additional anchor-point for the age of a star. We present here a complementary method that combines isochrones with an *empirical* gyrochronology model. The methodology is related to the van Saders et al. (2016) model in that both use a combination of rotation periods and other observable properties that track stellar evolution on the HRD in concert. The main difference is that the gyrochronology model used here is an entirely empirically calibrated one, as opposed to a physically derived one. One major advantage of using a physically motivated gyrochronology model is the ability to rely on physics to interpolate or extrapolate over parts of parameter space with sparse data coverage. However, rotational spin-down is a complex process that is not yet fully understood and currently no physical model can accurately reproduce all the data available. For this reason, even physically motivated gyrochronology models cannot always be used to reliably extrapolate into unexplored parameter space. Physical models, when calibrated to data, can provide insight into the physics of stars, however, if accurate and precise *prediction* of stellar properties is desired, empirical models can have advantages over physical ones. For example, the data may reveal complex trends that cannot be reproduced with our current understanding of the physical processes involved, but may be captured by more flexible data-driven models. In addition, it is relatively straightforward to build an element of stochasticity into empirical models, *i.e.* to allow for and incorporate outliers or noisy trends. This is particularly important for stellar spin down because rotation periods can be affected by additional confounding variables which are not always observed (having a binary or planetary companion, for example). A further advantage of empirical models is that inference is more tractable: it can be extremely fast to fit them to data.

In this work we calibrated a new empirical gyrochronology relation, fit to the Praesepe open cluster and the Sun. The Praesepe cluster has the largest number of measured rotation periods, spanning the largest mass range of any open cluster. This relation is a broken power law in $Gaia\ G_{BP} - G_{RP}$, that incorporates new rotation periods for late M dwarfs obtained with the $K2$ mission (Douglas et al. 2017; Rebull et al. 2017). We calibrated this new relation both to capture the detailed shape of its newly revealed rotation period-color relation and also to provide a gyrochronology relation calibrated to $Gaia\ G_{BP} - G_{RP}$ color. $Gaia\ G$, G_{BP} and G_{RP}-band apparent magnitudes are now the most widely available photometric measurements, with more than a billion stars from $Gaia$ DR2 (Gaia Collaboration et al. 2018). In fact, an important point of context for this work is the new availability of data relevant to gyrochronology and stellar ages. $Gaia$ now provides broad-band photometry and parallaxes for over a billion stars, and $Kepler, K2$ and $TESS$ are providing rotation periods for hundreds of thousands of stars. Gyrochronology is becoming one of the most readily available age-dating methods, so it is important to continue to improve gyrochronology relations and methods. Like any other gyrochronology model, this new Praesepe-based model cannot reproduce all the observed data and some simple modifications could make significant improvements, for example, by including a mixture model to account for outliers and binaries, and by removing the period-age, period-color separability to account for different period-color shapes seen in clusters of different ages. We leave these improvements for a future project and, for now, test this new Praesepe-based model which is built into an open source $Python$ package for gyrochronology, called `stardate`. `stardate` provides the framework for simultaneous gyrochronology and isochrone fitting, and, because `stardate` is modular, it would be straightforward to update the gyrochronology relation in future.

This paper is laid out as follows. In section 2 we describe our new age-dating model and its implementation, in section 3 we test this model on simulated stars and cluster stars, and in section 4 we discuss the implications of these tests and future pathways for development. Throughout this paper we use the term *'observables'* to refer to the following observed properties of a star, $T_{\rm eff}$, log(g), observed bulk metallicity ($[\hat{\rm Fe/}\rm H]$), parallax ($\bar{\omega}$), photometric colors in different passbands ($\mathbf{m_x} = [m_J, m_H, m_K, m_B, m_V, m_G, m_{GBP}, m_{GRP}...]$, etc) and rotation period ($P_{\rm rot}$). The term 'parameters' refers to the physical properties of that star: age (A), equivalent evolutionary point (EEP), true bulk metallicity (Fe/H), distance (D) and V-band extinction (A_V). These are the properties that generate the observables.

2. Method

We fit a broken power law to the 650 Myr Praesepe cluster in order to calibrate a new gyrochronology relation that takes advantage of new data available from the *K2* and *Gaia* surveys. Praesepe is the ideal calibration cluster because it has the largest number of members with precisely measured rotation periods, over a large range of colors (spanning spectral types A0 through M6), of any open cluster. It is relatively tightly clustered on the sky and many of its members were targeted in a single *K2* campaign, from which rotation periods have been measured via light curve frequency analysis (Douglas et al. 2017; Rebull et al. 2017). We compiled rotation periods, *Gaia* photometry and *Gaia* parallaxes for members of the 650 Myr Praesepe cluster (Fossati et al. 2008) by identifying Praesepe members with measured rotation periods from Douglas et al. (2017) in the *K2-Gaia* crossmatch catalog provided at `https://gaia-kepler.fun/`. This catalog cross-matched the EPIC catalog (Huber et al. 2016) with with the Gaia DR2 catalog (Gaia Collaboration et al. 2018), using a 1" search radius. The result was a sample of 757 stars with rotation periods, parallaxes and *Gaia* G, G_{BP} and G_{RP}-band photometry, shown in figure 1[12]. Although this new model does not perfectly describe the rotation period of every star, it provides a better representation of rotational evolution than previous models such as the Angus et al. (2015) model (as shown in figure 1). In order to fit a relation to Praesepe, we removed rotational outliers bluer than $G_{BP} - G_{RP} = 2.7$ via sigma-clipping and fit a 5th-order polynomial to the remaining FGK and early M stars. We also fit a straight line to the late M dwarfs ($G_{BP} - G_{RP} > 2.7$). We fit a separable straight line function to the period-age relation using the ages of Praesepe and the Sun[13]. This new Praesepe-calibrated gyrochronology relation is,

$$\log_{10}(P_{\rm rot}) = c_A \log_{10}(A) + \sum_{n=0}^{4} c_n [\log_{10}(G_{BP} - G_{RP})]^n \tag{1}$$

for stars with $G_{BP} - G_{RP} < 2.7$ and

$$\log_{10}(P_{\rm rot}) = c_A \log_{10}(A) + \sum_{m=0}^{1} b_m [\log_{10}(G_{BP} - G_{RP})]^m \tag{2}$$

for stars with $G_{BP} - G_{RP} > 2.7$, where $P_{\rm rot}$ is rotation period in days and A is age in years. Best-fit coefficient values are shown in table 1.

---

[12]This analysis was performed in a Jupyter notebook available here: `https://github.com/RuthAngus/stardate/blob/master/paper/code/Praesepe.ipynb`

[13]The fitting process was performed in a Jupyter notebook available at `https://github.com/RuthAngus/stardate/blob/master/paper/code/Fitting_Praesepe.ipynb`.

Fig. 1.— The rotation periods of Praesepe members (Douglas et al. 2016), vs. their *Gaia* colors $(G_{BP} - G_{RP})$ with a broken power law model, fit to these data. The dashed line and shaded region shows the mean and variance model described in equation 3 at 650 Myrs (lower model) and 4.56 Gyrs (upper model). The solid blue line shows the (Angus et al. 2015) gyrochronology relation at 650 Myrs (lower model) and 4.56 Gyrs (upper model). Shaded regions show the 1σ range of the log-normal rotation period model. The rotation periods of stars bluer than around 0.56 dex and redder than around 2.7 dex in $G_{BP} - G_{RP}$ are modelled as a broad log-normal distribution with a standard deviation of 0.5 dex, added to observational uncertainties. This figure was generated in a Jupyter notebook available at `https://github.com/RuthAngus/stardate/blob/master/paper/code/Fitting_Praesepe.ipynb`
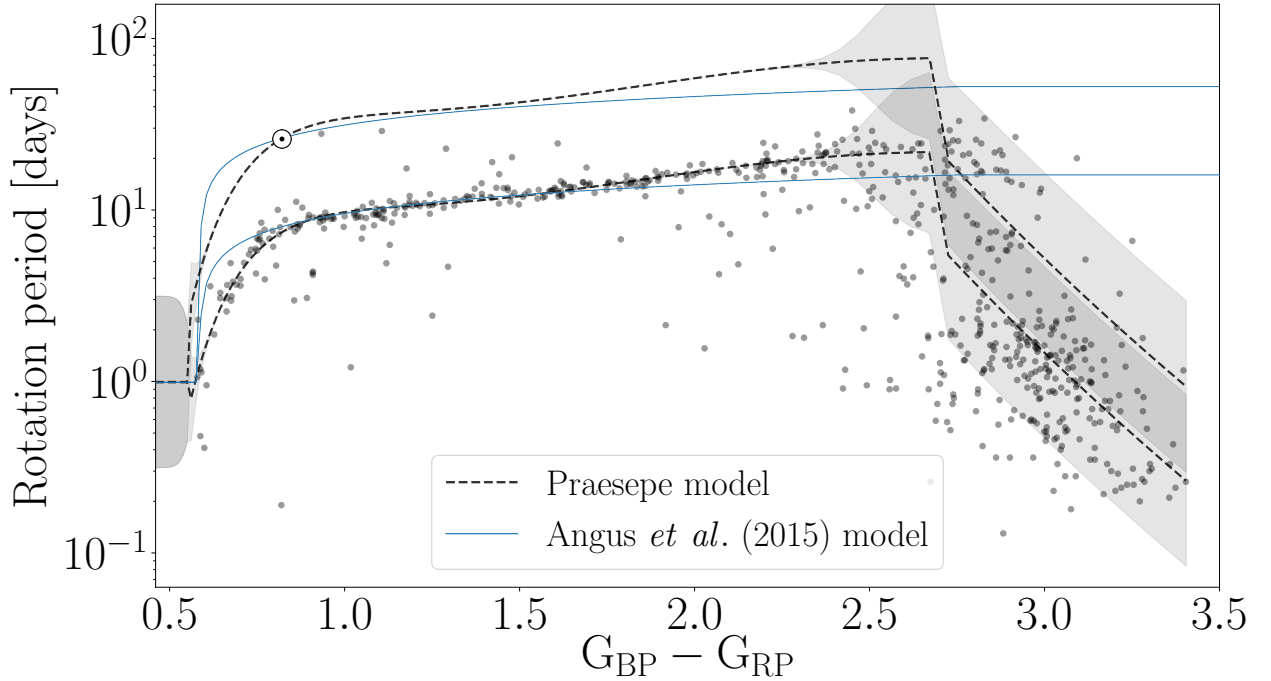
Table 1: Coefficient values for equations 1 and 2.

Coefficient	Value
c_A	0.65 ± 0.05
c_0	-4.7 ± 0.5
c_1	0.72 ± 0.05
c_2	-4.9 ± 0.2
c_3	29 ± 2
c_4	-38 ± 4
b_0	0.9 ± 0.5
b_1	-13.6 ± 0.1

We calibrated a new relation using Praesepe and the Sun alone, without including other clusters, because different open clusters have slightly different period-color relationships (Agüeros et al. 2018; Agüeros 2018; Curtis and Agüeros 2018) and, given that we use an age-color separable relation, adding in extra clusters is unlikely to improve the calibration in this format. We also did not include asteroseismic stars because they are slightly evolved and, since this gyrochronology relation does not include $\log g$, they are therefore not useful calibrators. This new relation, fit to Praesepe and the Sun, does not perfectly predict the rotation periods of stars at all colors and ages, but it provides several improvements over previous empirical gyrochronology relations. Firstly, it uses new *K2* rotation period measurements to model the period-color relation of Praesepe in detail, secondly, it includes a model for the rotational behavior of M dwarfs, and thirdly, it is calibrated to *Gaia* $G_{BP} - G_{RP}$ color: a directly observable quantity and the most widely available photometric color index. Equation 1 describes the rotational evolution of stars with Sun-like magnetic dynamos. These are stars that follow the Skumanich (1972) magnetic braking law, *i.e.* their rotation period increases with the square root of their age. It does not describe stars hotter than around 6250 K which have a thin convective layers and a weak magnetic dynamo, nor does it describe fully convective stars which take a long time to converge onto the Skumanich (1972) braking law. In addition, stars with Rossby numbers larger than around 2 do not show Skumanich-like magnetic braking (van Saders et al. 2016, 2018), so equation 1 does not describe these stars. It also does not describe the rotation periods of subgiants or giants, whose rotation periods are influenced by their expanding radii, changing winds, and core-to-surface differential rotation (*e.g.* van Saders and Pinsonneault 2013; Tayar and Pinsonneault 2018). Finally, this relation does not describe the rotation periods of dynamically or magnetically interacting binaries. Binaries often rotate more rapidly than isolated stars at the same age and color (Douglas et al. 2016).

In order to include non-Skumanich type stars in our combined gyrochronal and isochronal model, we designed a composite gyrochronology relation which describes a mean and variance model for the rotation period distributions across the HRD. Rotation periods are modeled differently for stars of different photometric color, EEP, Rossby number, age and metallicity. The rotation period model for each of these groups is described below.

- The rotation periods of late F, GK, and early M dwarfs are modeled as a log-normal distribution, with mean given by equation 1, and variance given by the squared inverse of the observational uncertainties.

- The rotation periods of stars with $G_{BP} - G_{RP} < 0.56$ dex are modeled with a log-normal distribution with mean, $\log_{10}(P_{\rm rot}) = 0.56$, and an extra standard deviation of 0.5 dex, added to observational uncertainties. Stars more massive than around 1.25 $M_\odot$, with a temperature $\gtrsim$ 6250 K and a $G_{BP} - G_{RP} \lesssim 0.56$ do not spin down appreciably over their main-sequence lifetimes because they do not have the deep convective envelope needed to generate strong magnetic fields. This model for the mean and variance of hot star rotation periods is based on stars hotter than 6250 K in the McQuillan et al. (2014) sample, which have a mean $\log_{10}(P_{\rm rot})$ of 0.56 dex and a standard deviation of around 0.5 dex.

- The rotation periods of fully convective stars ($G_{BP} - G_{RP} > 2.7$) are modeled with a log-normal distribution with mean given by equation 2, and additional standard deviation of 0.5 dex. This distribution reflects the observed rotation periods of late M dwarfs in the Praesepe cluster. Late M dwarfs with masses $\lesssim 0.3$ $M_\odot$, temperatures $\lesssim 3500$ and $G_{BP} - G_{RP} \gtrsim 2.7$ exhibit weak magnetic braking until at least after the age of Praesepe ($\sim$650 million years). Both hot and cool stars retain rotation periods that are similar to their primordial distribution (see e.g. Matt et al. 2012; Somers et al. 2017).

- The age at which a star's Rossby number would exceed 2 is calculated for each star by inverting equation 1. If a star's age is greater than this, its mean rotation period is given by $P_{\rm max} = 2/\tau$, where τ is the convective turnover timescale, calculated via stellar mass using equation 11 from Wright et al. (2011).

- The rotation periods of subgiants are described with a log-normal distribution with mean given by equation 1, 2 or 0.56, depending on its color, and an additional standard deviation of 0.5 dex. This is not strictly an accurate model of subgiant rotation periods (see, e.g. van Saders and Pinsonneault 2013) but, because of the inflated variance, it is a weakly constraining one. Isochrone fitting provides precise ages for subgiants, so

by inflating the variance of the gyrochronology relation at large EEP, we allow a star's position on the HRD/CMD to dominate the age information over its rotation period.

- We model stars younger than around 250 Myrs with a log-normal distribution with mean function given by 1, 2 or 0.56, depending on it whether it has an intermediate, blue or red color, respectively and a inflated standard deviation of 0.5 dex. Rotation periods in young open clusters show a large amount of scatter because they have not yet converged onto the Skumanich (1972) spin-down sequence.

- Finally, we model stars with very low and high metallicites (-3 < [Fe/H] < 3) with a log-normal distribution with mean given by 1, 2 or 0.56, depending on its color, and a standard deviation of 0.5 dex. Gyrochronology is not calibrated at these extreme metallicities due to a lack of suitable metal poor and rich calibration stars. Rather than assume the same gyrochronology model can be naïvely applied to these stars, we take a more conservative approach and model them with a broad Gaussian distribution.

Inflating the variance of the rotation period distribtion for stars with non-Skumanich magnetic braking behavior has two purposes: 1) in the cases of hot stars and fully convective stars, it allows the broad distributions of rotation periods observed in clusters and the field to be matched, and 2) it down-weights the age-information provided by rotation periods in regions of the HRD/CMD where rotation periods are not information-rich or the gyrochronology model is inaccurate or uncalibrated. If the observational uncertainties on rotation periods are 10% on average, which corresponds to $0.1/\ln(10) \sim 0.0434$ dex, adding 0.5 to this is a $12.5\times$ increase in standard deviation, or a $156\times$ increase in variance. The variance on stellar ages inferred via gyrochronology is directly proportional to the variance on rotation periods, so a $12.5\times$ increase in period standard deviation corresponds to a $12.5\times$ reduction in the age-information provide by gyrochronology and a $12.5\times$ increase in gyrochronal age uncertainty. So, practically speaking, when the standard deviation is inflated to 0.5 dex, ages are almost entirely inferred via isochrone fitting.

We used the following composite gyrochronology model to infer ages from rotation periods,

$$
\log_{10}(P_{\rm rot}) \sim \begin{cases} \mathcal{N}\left[(1), (\sigma + \sigma_P)^2\right], & Ro < 2, 0.56 < G_{BP} - G_{RP} < 2.7 \\ \mathcal{N}[(2), (\sigma + \sigma_P)^2], & Ro < 2, G_{BP} - G_{RP} > 2.7 \\ \mathcal{N}[\log_{10}(P_{\max}), (\sigma + \sigma_P)^2], & Ro \geq 2 \\ \mathcal{N}[0.56, (\sigma + \sigma_P)^2], & G_{BP} - G_{RP} < 0.56, \end{cases} \tag{3}
$$

where σ is the relative period uncertainty, divided by $\ln(10)$, on individual rotation period measurements and σ_P is an additional scatter that is a function of EEP, age, metallicity and

color. It takes a maximal value of 0.5 for hot stars, fully convective stars, subgiants and giants and a minimal value of zero for late F, GK and early M dwarfs. The variance model is shown in figure 2. Sigmoid functions were used to provide smooth transitions between regions of low and high variance. Sharp changes in variance would produce sharp changes in likelihood, which would cause the posterior distributions over stellar parameters to be more difficult to sample. The sigmoid functions shown in figure 2 reach half their maximum values at $G_{BP} - G_{RP} = 0.56$ and 2.5 for hot and cool stars respectively, EEP = 454 for subgiants age = 250 Myrs for young stars, [Fe/H] = -3 for metal poor stars and 3 for metal rich stars. The maximum additional standard deviation value (σ_P) is 0.5 for all stars and the minimum is zero. The logistic growth rate, or steepness, of the sigmoid functions is 100 dex^{-1} for both color transitions, .2 EEP^{-1} for the EEP transition, 20 dex^{-1} for the age transition and 5 dex^{-1} for the both metallicity transitions. The additional standard deviation is additive, so if a star is *e.g.* hot, evolved and metal poor, the additional standard deviation of its rotation period rises to 1.5.

The above part of this section describes the mean and variance relations we used to model the rotation periods of stars as a function of their ages (and colors, EEPs, masses and metallicities). In what follows, we describe how we combined this model with a stellar evolution model to infer stellar ages (and other parameters) via gyrochronology and isochrone fitting simultaneously. Our goal was to infer the age of a star from its observable properties by estimating the posterior probability density function (PDF) over age,

$$p(A|\mathbf{m_x}, P_{\text{rot}}, \bar{\omega}), \tag{4}$$

where A is age, $\mathbf{m_x}$ is a vector of apparent magnitudes in various bandpasses, P_{rot} is the rotation period and $\bar{\omega}$ is parallax. Spectroscopic properties (T_{eff}, log(g) and $\hat{\text{Fe/H}}$) and/or asteroseismic parameters ($\Delta\nu$ and ν_{max}) may also be available for a star, in which case they would appear to the right of the '|' in the above equation since they are observables. In order to calculate a posterior PDF over age, other stellar parameters must be marginalized over. These parameters are distance (D), V-band extinction (A_V), the inferred metallicity, F[14], and equivalent evolutionary point (abbreviated to EEP or E). EEP is a dimensionless number ranging from around 200 for M dwarfs up to around 800 for subgiants and is 355 for the Sun (see Dotter 2016; Choi et al. 2016). Stars are defined as subgiants when their EEP exceeds 454. Mass is uniquely defined by EEP, age and metallicity. The marginalization

---

[14]The inferred metallicity is a model parameter which is different to the *observed* metallicity which would appear on the right side of the '|$'$ in equation 4.

Fig. 2.— The additional rotation period scatter, σ_P, added to the observational period uncertainties in the model (see equation 3). The standard deviation is increased for early F and hotter stars ($G_{BP} - G_{RP} < 0.56$), late M dwarfs ($G_{BP} - G_{RP} > 2.7$) and evolved stars (EEP > 454) in order to down-weight the age-information supplied by rotation periods and reproduce observed rotation period distributions. We also increase the variance for stars younger than around 250 Myrs, because the rotation periods of these stars typically have not yet converged onto a tight gyrochronology sequence, and for very high and low metallicity stars (-3 $\lesssim$ [Fe/H] $\lesssim$ 3) because the gyrochronology relations have not been calibrated at these extreme values. Down-weighting the gyrochronal likelihood by the inverse variance ($1/\sigma^2$) allows the ages of these stars to be mostly inferred via isochrone fitting. Sigmoid functions were used to provide smooth transitions between regions of low and high variance.
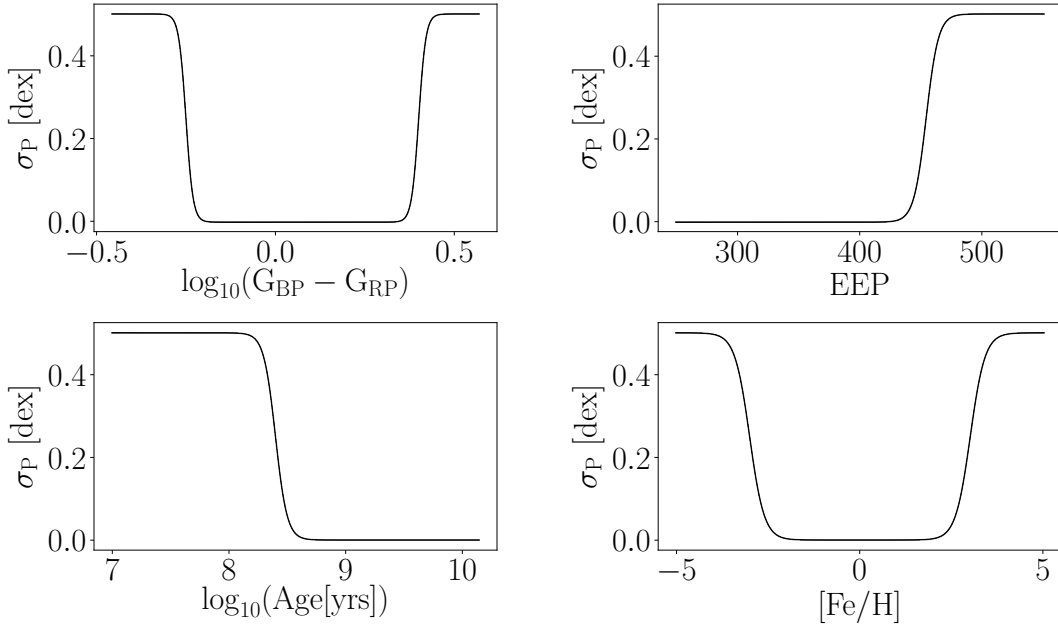
involves integrating over these extra parameters,

$$p(A|\mathbf{m_x}, P_{\text{rot}}, \bar{\omega}) \tag{5}$$
$$\propto \int p(\mathbf{m_x}, P_{\text{rot}}, \bar{\omega}|A, E, F, D, A_V) \ p(A)p(E)p(F)p(D)p(A_V)dEdFdDdA_V.$$

This equation is a form of Bayes' rule,

$$\text{Posterior} \propto \text{Likelihood} \times \text{Prior}, \tag{6}$$

where the likelihood of the data given the model is,

$$p(\mathbf{m_x}, \bar{\omega}, P_{\text{rot}}|A, E, D, A_V, F), \tag{7}$$

and the prior PDF over parameters is,

$$p(A)p(E)p(D)p(A_V)p(F). \tag{8}$$

The priors we used are described in the appendix.

The assumption of independence allowed us to multiply two separate likelihood functions together: one computed using an isochronal model and one computed using a gyrochronal model. We assumed that the probability of observing the measured observables, given the model parameters was a Gaussian and that the observables were identically and independently distributed. The isochronal likelihood function was,

$$\mathcal{L}_{\text{iso}} = p(\mathbf{m_x}, \bar{\omega}|A, E, F, D, A_V) \tag{9}$$
$$= \frac{1}{\sqrt{(2\pi)^n \det(\Sigma)}} \exp\left(-\tfrac{1}{2}(\mathbf{O_I} - \mathbf{I})^T \Sigma^{-1}(\mathbf{O_I} - \mathbf{I})\right),$$

where $\mathbf{O_I}$ is the vector of n observables: $\bar{\omega}$, $\mathbf{m_x}$ plus spectroscopic and/or asteroseismic observables if available, and Σ is the covariance matrix of that set of observables. $\mathbf{I}$ is the vector of *model* observables that correspond to a set of parameters: A, E, F, D and A_V, calculated using an isochrone model. We assumed there is no covariance between these observables and so this covariance matrix consists of individual parameter variances along the diagonal with zeros everywhere else. The gyrochronal likelihood function was,

$$\mathcal{L}_{\text{gyro}} = p(P_{\text{rot}}|A, E, F, D, A_V) \tag{10}$$
$$= \frac{1}{\sqrt{(2\pi) \det(\Sigma_P)}} \exp\left(-\tfrac{1}{2}(\mathbf{P_O} - \mathbf{P_P})^T \Sigma_P^{-1}(\mathbf{P_O} - \mathbf{P_P})\right),$$

where $\mathbf{P_O}$ is a 1-D vector of observed logarithmic rotation periods, and $\mathbf{P_P}$ is the vector of corresponding logarithmic rotation periods, predicted by the model. Σ_P was comprised of individual rotation period measurement uncertainties, plus an additional variance that is a

function of EEP and $G_{BP} - G_{RP}$ color, added in quadrature. This variance accounts for the stochastic nature of the rotation periods of very hot and very cool stars and allowed us to predominantly use isochrone fitting to measure the ages of subgiants. The full likelihood used in our model was the product of these two likelihood functions,

$$\mathcal{L}_{\text{full}} = \mathcal{L}_{\text{iso}} \times \mathcal{L}_{\text{gyro}}. \tag{11}$$

The inference processes proceeded as follows. First, a set of parameters: age, EEP, metallicity, distance and extinction, and observables for a single star were passed to the isochronal likelihood function in equation (9). Then, a set of observables corresponding to those parameters were generated from the MIST model grid using `isochrones.py` and compared to the measured observables via the isochronal likelihood, $\mathcal{L}_{\text{iso}}$ (also computed using `isochrones.py`. The parameters were also passed to the gyrochronology model (equation 3) where A, E, F, D and A_V were used to calculate $G_{BP} - G_{RP}$ color and mass from the MIST model grid and, in turn, rotation period via the gyrochronology model. EEP and $G_{BP} - G_{RP}$ were also used to calculate the additional rotation period variance, added to the individual period uncertainties. This model rotation period was compared to the measured rotation period using gyrochronal likelihood function of equation 10. The gyrochronal log-likelihood was added to the isochronal log-likelihood to give the full likelihood, which was then added to the log-prior to produce a single sample from the posterior PDF.

Ages were inferred with `stardate` using Markov Chain Monte Carlo. The joint posterior PDF over age, mass, metallicity, distance and extinction was sampled using the affine invariant ensemble sampler, `emcee` (Foreman-Mackey et al. 2013) with 24 walkers. Samples were drawn from the posterior PDF until 100 *independent* samples were obtained. We actively estimated the autocorrelation length, which indicates how many steps were taken per independent sample, after every 100 steps using the autocorrelation tool built into `emcee`. The MCMC concluded when *either* 100 times the autocorrelation length was reached and the change in autocorrelation length over 100 samples was less than 0.01, *or* the maximum of 100,000 samples was obtained. This method is trivially parallelizable, since the inference process for each star can be performed on a separate core. The age of a single star can be inferred in around 10 minutes on a laptop computer.

3. Results

In order to demonstrate the performance of our method, we conducted two sets of tests. In the first we simulated observables from a set of stellar parameters for a few hundred stars using the MIST stellar evolution models and the gyrochronology model of equation 3. The ages predicted with our model were compared to the true parameters used to generate the data. In the second we tested our model by measuring the ages of individual stars in the NGC 6819 open cluster.

3.1. Test 1: simulated stars

For the first test we drew masses, ages, bulk metallicities, distances and extinctions at random for 1000 stars from the following uniform distributions:

$$\text{EEP} \sim U(198, 480) \tag{12}$$

$$A \sim U(0.5, 14) \text{ [Gyr]} \tag{13}$$

$$F \sim U(-0.2, 0.2) \tag{14}$$

$$D \sim U(10, 1000) \text{ [pc]} \tag{15}$$

$$A_V \sim U(0, 0.1). \tag{16}$$

T_{eff}, log(g), $\hat{F}$, parallax, and apparent magnitudes B, V, J, H, K, $Gaia$ G, G_{BP} and G_{RP} were generated from these stellar parameters using the MIST stellar evolution models. We added a small amount of noise to the 'observed' stellar properties in order to reflect typical observational uncertainties. We added Gaussian noise with a standard deviation of 25 K to T_{eff}, 0.01 dex to [Fe/H] and log(g), and 10 mmags to B, V, J, H, and K magnitudes. The noise added to Gaia G-band photometry ranged from 0.3 mmag for stars brighter than 13th magnitude, to 10 mmag for stars around 20th magnitude (Evans et al. 2017; Gaia Collaboration et al. 2018). Noise added to $Gaia$ G_{BP} and G_{RP} bands ranged from 2 mmag for stars brighter than 13th magnitude to 200 mmag for stars fainter than 17th. Unphysical combinations of stellar parameters were discarded, resulting in a final sample size of 841 simulated stars. Figure 3 shows the position of these stars on an HRD (with log(g) on the y-axis instead of luminosity to improve the visibility of the MS), colored by their age. Rotation periods for FGK and early M dwarfs were generated using the gyrochronology relation of equation 3. Rotation periods for these stars were generated using the gyrochronology relation described in equation 3. We added a conservative value of 10% Gaussian noise to all stellar rotation periods. This is a rather crude approximation for the noise distribution of rotation periods which can be highly non-Gaussian (*e.g.* Aigrain et al. 2015; **?**). Figure 4 shows the

Fig. 3.— The simulated star sample plotted on an HRD, colored by age (top panel) and rotation period (bottom panel). HRD positions were calculated using MIST isochrones via the `isochrones.py` *Python* package and rotation periods were generated using equation 3. This figure was generated in a Jupyter notebook available at `https://github.com/RuthAngus/stardate/blob/master/paper/code/Simulate_data.ipynb`
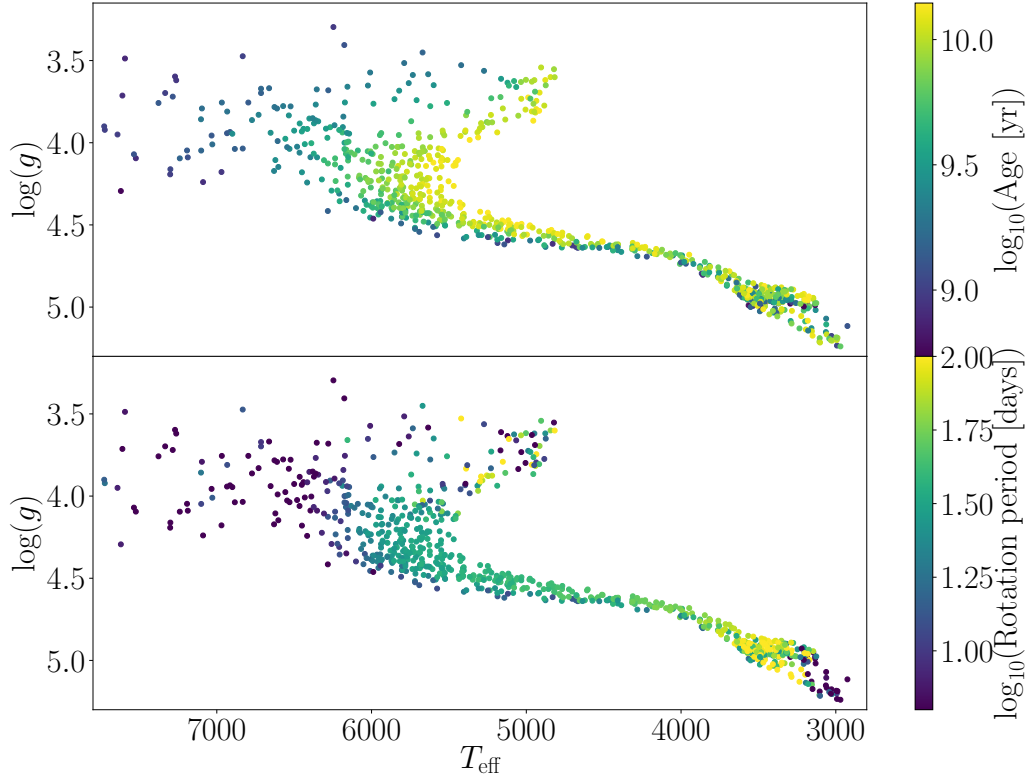
Fig. 4.— The rotation period model. Late F, GK and early M dwarfs (stars with $0.56 <$ $G_{BP}-G_{RP} < 2.7$ follow the Praesepe-calibrated gyrochronology relation (dashed gray lines), with the exception of old, slowly rotating stars with large Rossby numbers whose rotation periods are fixed at $2\times$ their convective overturn time. The rotation periods of early F ($G_{BP} - G_{RP} < 0.56$), late M dwarfs ($G_{BP} - G_{RP} < 2.7$) and subgiants (EEP > 454) were generated from a log-normal distribution with standard deviation shown in figure 2. The top panel shows the rotation periods vs. $G_{BP} - G_{RP}$ colors of simulated stars, colored by their age and the bottom panel shows the same stars colored by their equivalent evolutionary point (EEP). The gray lines describe the mean gyrochronology model at ages 1, 3, 5, 7, 9, 11, and 13 (rotation periods rise with age).
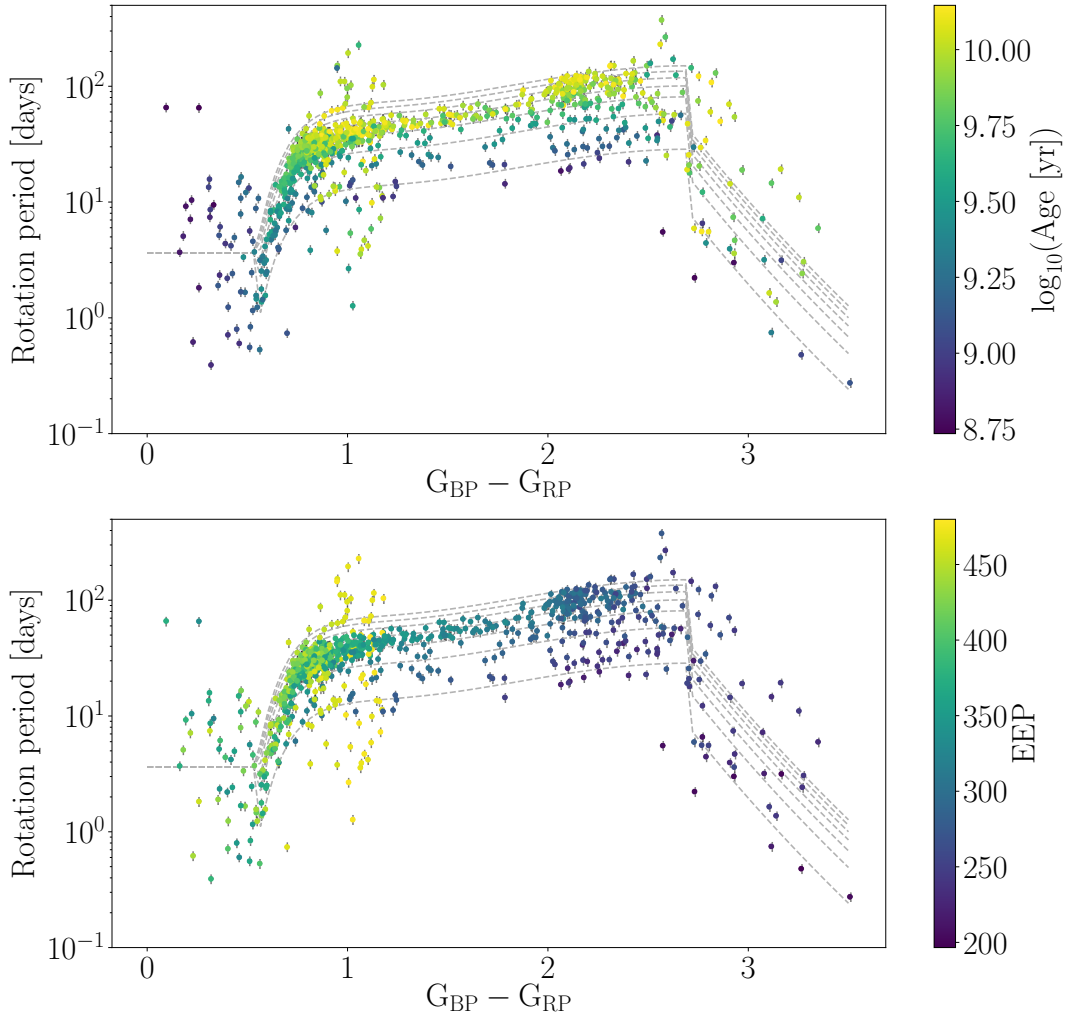
rotation periods of 841 stars generated from the gyrochronology model.

We took two approaches to inferring the ages of these simulated stars: firstly using isochrone fitting *only*, and secondly using isochrone fitting *combined with* a gyrochronology model (stardate). Since the posterior PDFs of stars are often not unimodal, we found that the choice of initial positions of the emcee walkers influenced the final outcome because walkers occasionally got stuck in local minima. We found that the following set of initial parameters worked well, though not perfectly, for FGK dwarfs but sacrificed some accuracy in subgiant ages: EEP = 330, $A = 9.56$ Gyr, $F = -0.05$, $D = 269$ pc and $A_V = 0.0$. Figure 5 shows the results of combining gyrochronology with isochrone fitting for the simulated sample. The stars' true ages are plotted against their predicted ages, with stardate ages in color, and ages predicted using isochrone fitting only plotted in light grey. The five panels show the results for five different types of stars: late F, GK and early M dwarfs which are still undergoing magnetic braking (Ro < 2), late F, GK and early M dwarfs that have ceased magnetic braking (Ro > 2), hot stars ($G_{BP} - G_{RP} < 0.56$), cool stars ($G_{BP} - G_{RP} > 2.7$) and evolved stars (EEP > 454). As expected, the low *Ro*, FGK stars show the most dramatic improvement in age precision. Summary statistics rewrite in progress...

Figure 6 shows the simulated stars on an HRD, with points colored by the relative precision of their predicted ages. The top panel shows the precision of ages calculated using both gyrochronology and isochrone fitting with stardate and the bottom panel shows the precision of ages calculated with isochrone fitting only. Although these uncertainties are noisy (they are computed from the standard deviation of the age posteriors) they show that combining gyrochronology and isochrone fitting improves age precision on the MS This simulation experiment is optimistic because data were simulated from the same gyrochronology model used to infer ages, so the results for FGK dwarfs are extremely accurate by design. stardate can provide precise ages with the caveat that the currently implemented gyrochronology model is not perfectly calibrated and ages will only be as accurate as the model.

3.2. Test 2: Open clusters

In order to test our model on real stars with known ages, we selected a sample of stars in the 2.5 Gyr NGC 6819 cluster. We compiled *Kepler*-based rotation periods (Meibom et al. 2015), *Gaia* photometry and *Gaia* parallaxes for members of the NGC 6819 cluster. Figure 7 shows the rotation period-color relation of this cluster and figure 8 shows the results of inferring the ages of individual cluster members using stardate and isochrone fitting. The ages of F stars in this cluster ($G_{BP} - G_{RP} \sim 5.5$-6.5) are relatively precisely constrained by

Fig. 5.— The true vs. predicted ages of simulated stars. Ages calculated by combining gyrochronology and isochrone fitting with `stardate` are shown in color and ages calculated with isochrone fitting only are shown in gray. The five panels show the results for five different groups of stars: low Ro late F, GK and early M dwarfs, high Ro late F, GK and early M dwarfs, early F stars ($G_{BP} - G_{RP} < 0.56$), late M dwarfs ($G_{BP} - G_{RP} > 2$) and subgiants (EEP > 454). Gyrochronology is highly effective for low Ro late F, GK and early M dwarfs and somewhat effective for high Ro late F, GK and early M dwarfs. Ages for other groups were improved slightly but not substantially.
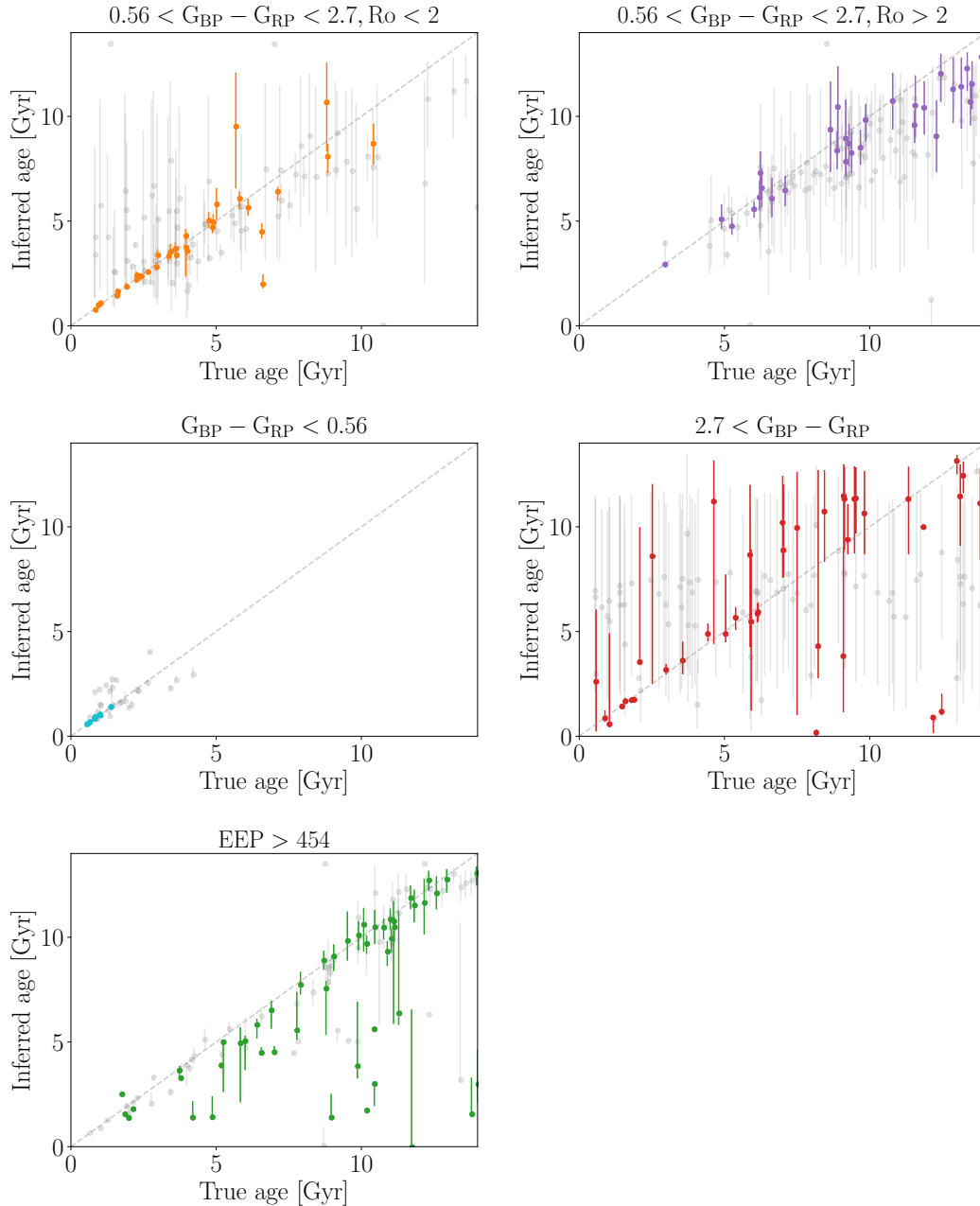
Fig. 6.— Simulated stars on an HRD, colored by their relative age precision using gyrochronology and isochrone fitting via `stardate` (top panel) and isochrone fitting only (bottom panel). Combining gyrochronology with isochrone fitting significantly improves stellar age precision on the MS. Isochrone fitting provides precise ages for hot stars and subgiants and the rotation periods of these stars are relatively uninformative, so gyrochronology does not significantly improve their age precision. The ages of late M dwarfs are highly imprecise because their ages are not well determined by either their rotation periods or their position on the HRD or CMD.
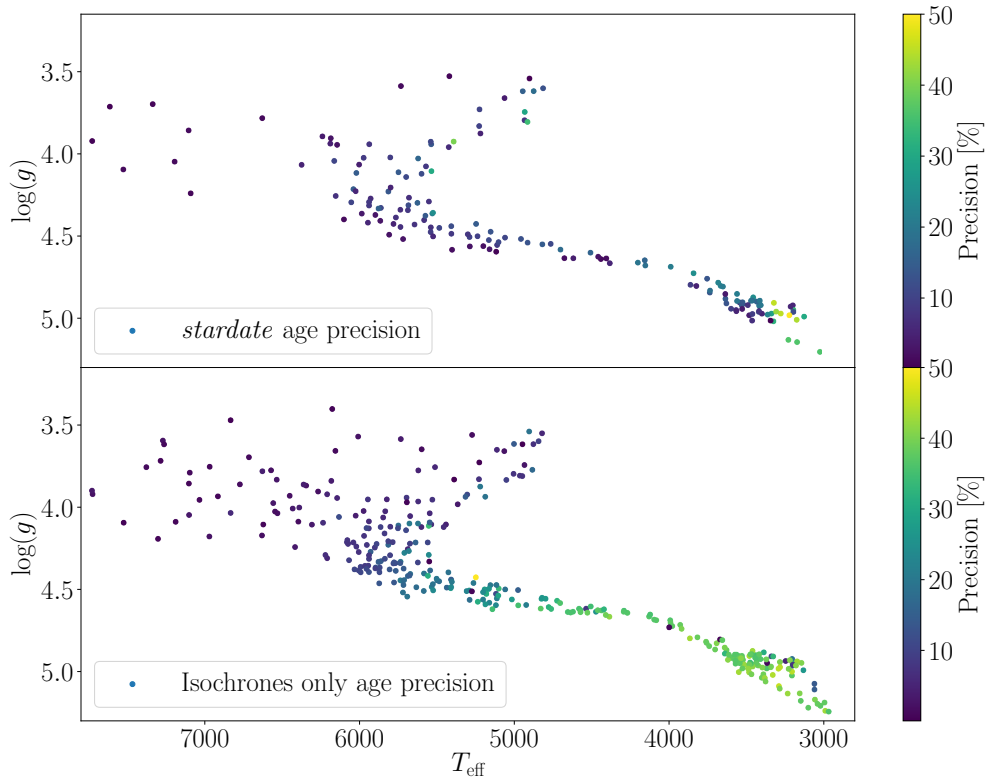
isochrone fitting alone because, at 2.5 Gyr, they are approaching MS turn-off. The `stardate` and isochrone-only ages are consistent for this group of stars and similarly precise, showing that isochrones provide a lot of age information for these stars and rotation periods do not add significantly more information. The G and early K stars in this cluster ($G_{BP} - G_{RP}$ $\lesssim 6.5$) are not precisely recovered from isochrone fitting alone – the isochrone-only age posteriors tend towards the prior which is a uniform distribution between 0 and 13.8 Gyrs. In contrast, the rotation periods of G and K stars in this cluster significantly improve the accuracy of age measurements. The median age of stars in this cluster was 2.63 ± 0.16 Gyr when ages were inferred with a combination of isochrone fitting and gyrochronology, with a Praesepe-calibrated gyrochronology model. The previously-calibrated Angus et al. (2015) model resulted in a median age of 2.66 ± 0.21 Gyr. The median age of the cluster, calculated with isochrone fitting and a Praesepe-calibrated gyrochronology model, without correcting the photometry for redenning, was slightly under-estimated at 1.86 ± 0.22 Gyr. This suggests that, despite the fact that V-band extinction is a parameter that gets marginalized over during the inference process, correcting for extinction *before* ages are estimated will reduce bias introduced by dust. Finally, the median age of stars in the cluster was 4.27 ± 0.48 Gyr when only isochrone fitting was used. Isochrone-only ages were over-estimated because they were prior dominated, and the prior was a uniform distribution between 0 and 13.8 Gyr.

We found that 5% rotation period uncertainties resulted in the most accurate ages for NGC 6819. The uncertainties on the measured rotation periods, provided in Meibom et al. (2015) and shown in figure 7, were underestimated for some stars. Underestimating the rotation period uncertainty can result in an inaccurate age estimate. This raises the question: how should uncertainties on rotation periods be estimated? The likelihood is weighted by the inverse variance, so uncertainties on the rotation period control the relative information provided by gyrochronology, isochrones, and the prior. If rotation period uncertainties are either too large or too small, the resulting age estimate will be imprecise and/or inaccurate. It is difficult to measure uncertainties on rotation periods directly because standard techniques such as Lomb-Scargle periodograms and autocorrelation functions do not have a reliable way to calculate realistic uncertainties. In general, rotation period uncertainties should probably be calculated empirically via simulations as in the Aigrain et al. (2015) study. A thorough exploration of how rotation period uncertainties affect stellar ages via gyrochronology would be useful in future.

Fig. 7.— The *Kepler*-based rotation periods of members of the 2.5 Gyr NGC 6819 open cluster. The raw $G_{BP} - G_{RP}$ colors are shown in red and the dust-corrected colors are shown in black. The dashed line shows a gyrochronology model that was fit to the Praesepe cluster and the Sun in this work, interpolated to 2.5 Gyrs. This model was used to infer the ages of these stars. For comparison, the solid blue line shows a previously calibrated gyrochronology model (Angus et al. 2015).
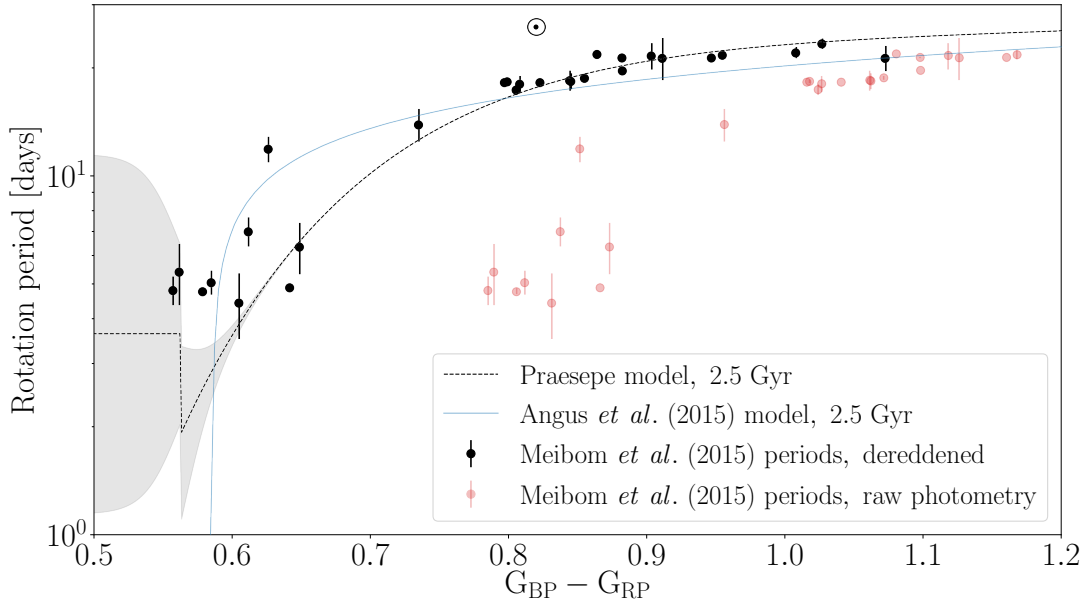
Fig. 8.— The inferred ages of members of the NGC 6819 open cluster as a function of their $G_{BP} - G_{RP}$ color. Black circles and red squares show the ages of stars inferred using a combination of isochrone fitting and gyrochronology, with a gyrochronology relation that was calibrated to Praesepe and the Sun. Black circles show ages inferred with dereddened *Gaia G*, G_{BP} and G_{RP} photometry and red squares show ages inferred with uncorrected, raw, photometry. Even though V-band extinction is marginalized over in the inference process, reddening can still bias ages. Blue triangles, pointing down show ages inferred using isochrone fitting and gyrochronology, with the Angus et al. (2015) gyrochronology model. Orange triangles show ages inferred using isochrone fitting only. The ages of F stars (stars bluer than 0.7) were precisely constrained by isochrones and including gyrochronology makes little difference to their inferred ages. The ages of G and K dwarfs (stars redder than 0.7) were improved in both precision and accuracy by including gyrochronology. The average age of stars, inferred using the gyrochronology model calibrated to Praesepe and the Sun (black circles) was 2.65 ± 0.13 which is consistent with the established cluster age.
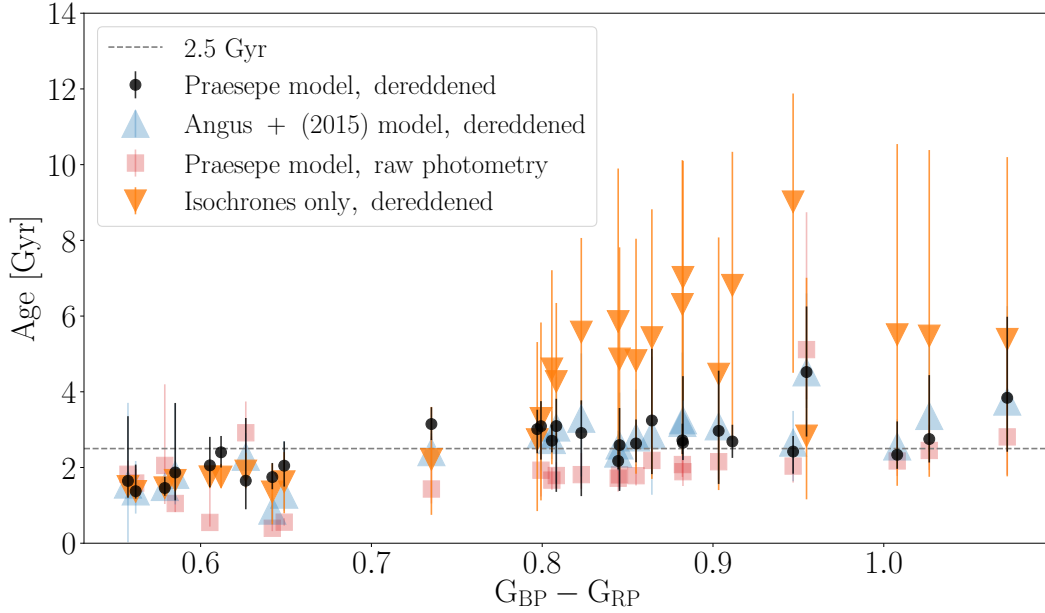
4. Conclusion

We present a statistical framework for measuring precise ages of MS stars and subgiants by combining observables that relate, via different evolutionary processes, to stellar age. Specifically, we combined HRD/CMD placement with rotation periods, in a hierarchical Bayesian model, to age-date stars based on both their hydrogen burning and magnetic braking history. The two methods of isochrone fitting and gyrochronology were combined by taking the product of two likelihoods: one that contains an isochronal model and the other a gyrochronal one. We used the MIST stellar evolution models and computed isochronal ages and likelihoods using the `isochrones.py` *Python* package. We fit a new broken power law gyrochronology model to the Praesepe cluster and included a modification recommended by van Saders et al. (2016) that accounts for weakened magnetic braking at Rossby numbers larger than 2. The rotation periods of hot stars, cool stars, evolved stars, young stars and extremely metal poor and rich stars were modeled stochastically with a broad log-normal distribution. We tested `stardate` on simulated data and cluster stars and demonstrated that combining gyrochronology with isochrone fitting increases the precision of age estimates, compared to using isochrone fitting alone.

`stardate` may predict inaccurate ages for stars in close binaries whose interactions influence their rotation period evolution. Rotational outliers are often seen in clusters (see *e.g.* Douglas et al. 2016; Rebull et al. 2016; Douglas et al. 2017; Rebull et al. 2017) and many of these fall above the main sequence on a CMD, indicating that they are binaries. In addition, measured rotation periods may not always be accurate and can, in many cases, be a harmonic of the true rotation period. For example, a common rotation period measurement failure mode is to measure half the true rotation period. The best way to prevent an erroneous or outlying rotation period from resulting in an erroneous age measurement is to *allow* for outlying rotation periods using a mixture model, and we intend to build a mixture model into `stardate` in future.

The optimal way to age-date stars is by combining *all* their available age-related observables. This could ultimately include activity dating via flare rates and chromospheric activity indices, kinematic dating and chemical dating. Of all the established age-dating methods, gyrochronology and isochrone fitting are two of the most complementary. The two methods are optimal in different parts of the HRD: gyrochronology works well for FGK dwarfs and isochrone fitting works well for subgiants and hot stars, so combining the two methods results in consistently precise ages across a range of masses, ages and evolutionary stages. In addition, using both methods at once circumvents the need to decide which method to use *a priori*. It eliminates the circular process of classifying a star based on its CMD position (M dwarf, subgiant, etc), then deciding which age-dating method to use, then

inferring an age which itself depends on the classification that was made. It is important to infer all stellar properties at once since they all depend on each other. stardate is applicable to a large number of stars: AFGKM dwarfs and subgiants with a rotation period and broad-band photometry. This already includes tens-of-thousands of *Kepler* and *K2* stars and could include millions more from *TESS*, *LSST*, *WFIRST*, *PLATO*, *Gaia*, and others in future.

The code used in this project is available as a *python* package called stardate. It is available for download via Github[15] or through PyPI[16]. Documentation is available at https://stardate.readthedocs.io/en/latest/. All code used to produce the figures in this paper is available at https://github.com/RuthAngus/stardate. add github hash and Zenodo doi.

---

[15]git clone https://github.com/RuthAngus/stardate.git

[16]pip install stardate_code

5. Appendix

Priors

We used the default priors in the `isochrones.py` *python* package. The prior over age was,

$$p(A) = \frac{\log(10)10^A}{10^{10.5} - 10^8}, \quad 8 < A < 10.5. \tag{17}$$

where A, is $\log_{10}(\mathrm{Age\ [yrs]})$. The prior over EEP was uniform with an upper limit of 800. We found that adding this upper limit reduced some multi-modality caused by the giant branch and resulted in better performance. The prior over true bulk metallicity was based on the galactic metallicity distribution, as inferred using data from the Sloan Digital Sky Survey (Casagrande et al. 2011). It is the product of a Gaussian that describes the metallicity distribution over halo stars and two Gaussians that describe the metallicity distribution in the thin and thick disks:

$$p(F) = \qquad H_F \frac{1}{\sqrt{2\pi\sigma_{\mathrm{halo}}^2}} \exp\left(-\frac{(F-\mu_{\mathrm{halo}})^2}{2\sigma_{\mathrm{halo}}}\right) \tag{18}$$
$$\times (1-H_F)\frac{1}{\xi}\left[\frac{0.8}{0.15}\exp\left(-\frac{(F-0.016)^2}{2\times 0.15^2}\right) + \frac{0.2}{0.22}\exp\left(-\frac{(F-0.15)^2}{2\times 0.22^2}\right)\right],$$

where $H_F = 0.001$ is the halo fraction, μ_{halo} and σ_{halo} are the mean and standard deviation of a Gaussian that describes a probability distribution over metallicity in the halo, and take values -1.5 and 0.4 respectively. The two Gaussians inside the square brackets describe probability distributions over metallicity in the thin and thick disks. The values of the means and standard deviations in these Gaussians are from Casagrande et al. (2011). ξ is the integral of everything in the square brackets from $-\infty$ to ∞ and takes the value ~ 2.507. The prior over distance was,

$$p(D) = \frac{3}{3000^3}D^2, \quad 0 < D < 3000, \tag{19}$$

with D in kiloparsecs, and, finally, the prior over extinction was uniform between zero and one,

$$p(A_V) = U(0, 1). \tag{20}$$

REFERENCES

M. A. Agüeros, E. C. Bowsher, J. J. Bochanski, P. A. Cargile, K. R. Covey, S. T. Douglas, A. Kraus, A. Kundert, N. M. Law, A. Ahmadi, and H. G. Arce. A New Look at an Old Cluster: The Membership, Rotation, and Magnetic Activity of Low-mass Stars in the 1.3 Gyr Old Open Cluster NGC 752. *ApJ*, 862(1):33, Jul 2018. doi: 10.3847/1538-4357/aac6ed.

Marcel Agüeros. The evolution of cool dwarf spin rates: Data, models, and tensions. In *Cambridge Workshop on Cool Stars, Stellar Systems, and the Sun*, Cambridge Workshop on Cool Stars, Stellar Systems, and the Sun, page 17, Jul 2018. doi: 10.5281/zenodo.1343628.

S. Aigrain, J. Llama, T. Ceillier, M. L. das Chagas, J. R. A. Davenport, R. A. García, K. L. Hay, A. F. Lanza, A. McQuillan, T. Mazeh, J. R. de Medeiros, M. B. Nielsen, and T. Reinhold. Testing the recovery of stellar rotation signals from Kepler light curves using a blind hare-and-hounds exercise. *MNRAS*, 450(3):3211–3226, Jul 2015. doi: 10.1093/mnras/stv853.

R. Angus, S. Aigrain, D. Foreman-Mackey, and A. McQuillan. Calibrating gyrochronology using Kepler asteroseismic targets. *MNRAS*, 450:1787–1798, June 2015. doi: 10.1093/mnras/stv423.

S. A. Barnes. On the Rotational Evolution of Solar- and Late-Type Stars, Its Magnetic Origins, and the Possibility of Stellar Gyrochronology. *ApJ*, 586:464–479, March 2003. doi: 10.1086/367639.

S. A. Barnes. Ages for Illustrative Field Stars Using Gyrochronology: Viability, Limitations, and Errors. *ApJ*, 669:1167–1189, November 2007. doi: 10.1086/519295.

L. Casagrande, R. Schönrich, M. Asplund, S. Cassisi, I. Ramírez, J. Meléndez, T. Bensby, and S. Feltzing. New constraints on the chemical evolution of the solar neighbourhood and Galactic disc(s). Improved astrophysical parameters for the Geneva-Copenhagen Survey. *A&A*, 530:A138, Jun 2011. doi: 10.1051/0004-6361/201016276.

J. Choi, A. Dotter, C. Conroy, M. Cantiello, B. Paxton, and B. D. Johnson. Mesa Isochrones and Stellar Tracks (MIST). I. Solar-scaled Models. *ApJ*, 823:102, June 2016. doi: 10.3847/0004-637X/823/2/102.

Jason Curtis and Marcel Agüeros. Problems with and Prospects for K dwarf Gyrochronology: Insights from the K2 Survey of Ruprecht 147. In *Cambridge Workshop on Cool Stars,*

Stellar Systems, and the Sun, Cambridge Workshop on Cool Stars, Stellar Systems, and the Sun, page 24, Jul 2018. doi: 10.5281/zenodo.1403719.

A. Dotter. MESA Isochrones and Stellar Tracks (MIST) 0: Methods for the Construction of Stellar Isochrones. *ApJS*, 222:8, January 2016. doi: 10.3847/0067-0049/222/1/8.

A. Dotter, B. Chaboyer, D. Jevremović, V. Kostov, E. Baron, and J. W. Ferguson. The Dartmouth Stellar Evolution Database. *ApJS*, 178:89–101, September 2008. doi: 10.1086/589654.

S. T. Douglas, M. A. Agüeros, K. R. Covey, P. A. Cargile, T. Barclay, A. Cody, S. B. Howell, and T. Kopytova. K2 Rotation Periods for Low-mass Hyads and the Implications for Gyrochronology. *ApJ*, 822:47, May 2016. doi: 10.3847/0004-637X/822/1/47.

S. T. Douglas, M. A. Agüeros, K. R. Covey, and A. Kraus. Poking the Beehive from Space: K2 Rotation Periods for Praesepe. *ApJ*, 842:83, June 2017. doi: 10.3847/1538-4357/aa6e52.

D. W. Evans, M. Riello, F. De Angeli, G. Busso, F. van Leeuwen, C. Jordi, C. Fabricius, A. G. A. Brown, J. M. Carrasco, H. Voss, M. Weiler, P. Montegriffo, C. Cacciari, P. Burgess, and P. Osborne. Gaia Data Release 1. Validation of the photometry. *A&A*, 600:A51, April 2017. doi: 10.1051/0004-6361/201629241.

D. Foreman-Mackey, D. W. Hogg, D. Lang, and J. Goodman. emcee: The MCMC Hammer. *PASP*, 125:306, March 2013. doi: 10.1086/670067.

L. Fossati, S. Bagnulo, J. Landstreet, G. Wade, O. Kochukhov, R. Monier, W. Weiss, and M. Gebran. The effect of rotation on the abundances of the chemical elements of the A-type stars in the Praesepe cluster. *A&A*, 483:891–902, June 2008. doi: 10.1051/0004-6361:200809467.

Gaia Collaboration, A. G. A. Brown, A. Vallenari, T. Prusti, J. H. J. de Bruijne, C. Babusiaux, C. A. L. Bailer-Jones, M. Biermann, D. W. Evans, L. Eyer, and et al. Gaia Data Release 2. Summary of the contents and survey properties. *A&A*, 616:A1, August 2018. doi: 10.1051/0004-6361/201833051.

F. Gallet and J. Bouvier. Improved angular momentum evolution model for solar-like stars. II. Exploring the mass dependence. *A&A*, 577:A98, May 2015. doi: 10.1051/0004-6361/201525660.

Daniel Huber, Stephen T. Bryson, Michael R. Haas, Thomas Barclay, Geert Barentsen, Steve B. Howell, Sanjib Sharma, Dennis Stello, and Susan E. Thompson. The K2

Ecliptic Plane Input Catalog (EPIC) and Stellar Classifications of 138,600 Targets in Campaigns 1-8. *The Astrophysical Journal Supplement Series*, 224:2, May 2016. doi: 10.3847/0067-0049/224/1/2.

J. Irwin and J. Bouvier. The rotational evolution of low-mass stars. In E. E. Mamajek, D. R. Soderblom, and R. F. G. Wyse, editors, *The Ages of Stars*, volume 258 of *IAU Symposium*, pages 363–374, June 2009. doi: 10.1017/S1743921309032025.

S. D. Kawaler. Angular momentum loss in low-mass stars. *ApJ*, 333:236–247, October 1988. doi: 10.1086/166740.

S. D. Kawaler. Rotational dating of middle-aged stars. *ApJ*, 343:L65–L68, August 1989. doi: 10.1086/185512.

E. E. Mamajek and L. A. Hillenbrand. Improved Age Estimation for Solar-Type Dwarfs Using Activity-Rotation Diagnostics. *ApJ*, 687:1264–1293, November 2008. doi: 10. 1086/591785.

S. P. Matt, K. B. MacGregor, M. H. Pinsonneault, and T. P. Greene. Magnetic Braking Formulation for Sun-like Stars: Dependence on Dipole Field Strength and Rotation Rate. *ApJ*, 754:L26, August 2012. doi: 10.1088/2041-8205/754/2/L26.

S. P. Matt, A. S. Brun, I. Baraffe, J. Bouvier, and G. Chabrier. The Mass-dependence of Angular Momentum Evolution in Sun-like Stars. *ApJ*, 799:L23, January 2015. doi: 10.1088/2041-8205/799/2/L23.

A. McQuillan, T. Mazeh, and S. Aigrain. Rotation Periods of 34,030 Kepler Main-sequence Stars: The Full Autocorrelation Sample. *ApJS*, 211:24, April 2014. doi: 10.1088/ 0067-0049/211/2/24.

S. Meibom, S. A. Barnes, I. Platais, R. L. Gilliland, D. W. Latham, and R. D. Mathieu. A spin-down clock for cool stars from observations of a 2.5-billion-year-old cluster. *Nature*, 517:589–591, January 2015. doi: 10.1038/nature14118.

Frédéric Pont and Laurent Eyer. Isochrone ages for field dwarfs: method and application to the age-metallicity relation. *MNRAS*, 351(2):487–504, Jun 2004. doi: 10.1111/j. 1365-2966.2004.07780.x.

L. M. Rebull, J. R. Stauffer, J. Bouvier, A. M. Cody, L. A. Hillenbrand, D. R. Soderblom, J. Valenti, D. Barrado, H. Bouy, D. Ciardi, M. Pinsonneault, K. Stassun, G. Micela, S. Aigrain, F. Vrba, G. Somers, J. Christiansen, E. Gillen, and A. Collier Cameron. Rotation in the Pleiades with K2. I. Data and First Results. *AJ*, 152:113, November 2016. doi: 10.3847/0004-6256/152/5/113.

L. M. Rebull, J. R. Stauffer, L. A. Hillenbrand, A. M. Cody, J. Bouvier, D. R. Soderblom, M. Pinsonneault, and L. Hebb. Rotation of Late-type Stars in Praesepe with K2. *ApJ*, 839:92, April 2017. doi: 10.3847/1538-4357/aa6aa4.

A. Skumanich. Time Scales for CA II Emission Decay, Rotational Braking, and Lithium Depletion. *ApJ*, 171:565, February 1972. doi: 10.1086/151310.

Garrett Somers, John Stauffer, Luisa Rebull, Ann Marie Cody, and Marc Pinsonneault. M Dwarf Rotation from the K2 Young Clusters to the Field. I. A Mass-Rotation Correlation at 10 Myr. *ApJ*, 850(2):134, Dec 2017. doi: 10.3847/1538-4357/aa93ed.

Jamie Tayar and Marc H. Pinsonneault. Testing Angular Momentum Transport and Wind Loss in Intermediate-mass Core-helium Burning Stars. *ApJ*, 868(2):150, Dec 2018. doi: 10.3847/1538-4357/aae979.

J. L. van Saders and M. H. Pinsonneault. Fast Star, Slow Star; Old Star, Young Star: Subgiant Rotation as a Population and Stellar Physics Diagnostic. *ApJ*, 776:67, October 2013. doi: 10.1088/0004-637X/776/2/67.

J. L. van Saders, T. Ceillier, T. S. Metcalfe, V. Silva Aguirre, M. H. Pinsonneault, R. A. García, S. Mathur, and G. R. Davies. Weakened magnetic braking as the origin of anomalously rapid rotation in old field stars. *Nature*, 529:181–184, January 2016. doi: 10.1038/nature16168.

J. L. van Saders, M. H. Pinsonneault, and M. Barbieri. Forward Modeling of the Kepler Stellar Rotation Period Distribution: Interpreting Periods from Mixed and Biased Stellar Populations. *ArXiv e-prints*, March 2018.

N. J. Wright, J. J. Drake, E. E. Mamajek, and G. W. Henry. The Stellar-activity-Rotation Relationship and the Evolution of Stellar Dynamos. *ApJ*, 743:48, December 2011. doi: 10.1088/0004-637X/743/1/48.

S. Yi, P. Demarque, Y.-C. Kim, Y.-W. Lee, C. H. Ree, T. Lejeune, and S. Barnes. Toward Better Age Estimates for Stellar Populations: The Y^2 Isochrones for Solar Mixture. *ApJS*, 136:417–437, October 2001. doi: 10.1086/321795.